ELSEVIER

Chemical Engineering Journal 90 (2002) 97–106

Chemical Engineering Journal

www.elsevier.com/locate/cej

# Short contact time catalytic partial oxidation of methane: analysis of transport phenomena effects

M. Bizzi [a], L. Basini [b], G. Saracco [a,*], V. Specchia [a]

[a] *Department of Materials Science and Chemical Engineering, Politecnico di Torino, C.so Duca degli Abruzzi 24, 10129 Torino, Italy*
[b] *Snamprogetti S.p.A., Via Maritano 26, 20097 San Donato, Milanese, Italy*

**Abstract**

The physico-chemical features of short contact time catalytic partial oxidation (SCT-CPO) of methane to produce synthesis gas have been examined with experimental and theoretical modelling activities. The experiments have been performed in a fixed bed reactor equipped with IR thermography and thermocouples for a detailed temperature mapping of the solid and of the gas phases. The theoretical analysis has been developed considering a diffusion–reaction system where transport phenomena and chemical kinetics have been coupled and it has been demonstrated that in the reaction system, a transfer controlled operating regime is established where the oxygen transport from the bulk gas phase to the catalyst is the rate limiting step and where local temperature differences are originated between the solid phase surface and the gas phase.


*Keywords:* Catalytic partial oxidation; Synthesis gas; Short contact time reactors; Reaction and mass–heat transport modelling; Infrared thermography experiments; Rhodium based catalyst

## 1. Introduction

The technology for the conversion of hydrocarbons sources (natural gas, naphtha, heavy oils, etc.) into synthesis gas has been known and applied in the last 60 years. However, syngas production is energy and capital intensive, and improvements are continuously pursued.

Currently, steam reforming (SR), non-catalytic partial oxidation (PO), autothermal reforming (ATR) and combined reforming (CR) processes have reached a considerable level of development and their main topics are described in several literature reviews [1–6].

In parallel to the efforts devoted to the improvements of the existing processes, great attention has been addressed towards the definition of new ways of producing synthesis gas.

One of the most successful approaches has been initiated in 1992 both in academic [7,8] and industrial fields, and a direct short contact time catalytic partial oxidation (SCT-CPO) of the hydrocarbons is employed. In this case, the synthesis gas is obtained by passing the reactants for few milliseconds inside a small volume catalytic bed and producing the main synthesis gas components, namely $H_2$ and CO, through direct mildly exothermic partial oxidation reactions.

This approach has been widely investigated both in its fundamental [9–18] and technological aspects [19]. It has been developed by Shell, and recently by a joint team of Haldor Topsoe A/S and Snamprogetti S.p.A. researchers, that has designed the first pilot plant which demonstrates this technology at a semi-industrial scale. The construction of the plant has been completed in Huston, USA and studies are currently in progress for the development of an industrial unit.

Most of the work in the literature of SCT-CPO of methane were carried out on monolithic reactors. However, a recent study [20] has shown that fixed bed reactors, despite their minor importance in the literature, offer superior performance especially in terms of stability of operation. This work presents experimental and theoretical activities on SCT-CPO of methane on a fixed bed reactor of rhodium coated alumina particles. First, a set of experimental data is presented, consisting of conversion, selectivity and thermal profiles at different space velocities. These data provide the necessary basis for extensive modelling activities of fixed bed reactors, that are currently underway. The experimental data revealed the typical features of the systems under the control of transport phenomena. Therefore, a theoretical analysis is formulated to support the proposed interpreta-

* Corresponding author. Tel.: +39-011-5644654; fax: +39-011-5644699.
*E-mail address:* saracco@polito.it (G. Saracco).

1385-8947/02/$ – see front matter 
PII: S1385-8947(02)00071-2

**Nomenclature**

| | |
|---|---|
| $a$ | surface to volume ratio ($m^{-1}$) |
| $c$ | molar concentration ($mol\,cm^{-3}$) |
| $d_p$ | particle diameter (m) |
| $D$ | diffusivity ($m^2\,s^{-1}$) |
| $Da_s$ | superficial Damkohler number |
| $f_{EN}$ | mass transfer enhancement factor |
| $G$ | specific mass flow rate ($kg\,s^{-1}\,m^{-2}$) |
| $h$ | heat transfer coefficient ($J\,K^{-1}\,m^{-2}\,s^{-1}$) |
| $\hat{H}_i$ | enthalpy of the species $i$ ($J\,g^{-1}$) |
| $J$ | mass transfer flux ($mol\,m^{-2}\,s^{-1}$) |
| $J_D$ | mass transfer factor |
| $J_H$ | heat transfer factor |
| $k_x$ | mass transfer coefficient ($m\,s^{-1}$) |
| $k'$ | first-order kinetic constant of a surface phase reaction ($m\,s^{-1}$) |
| KK | total number of chemical species involved in the reaction environment |
| $M$ | mole weight of species $i$ ($g\,mol^{-1}$) |
| $R_{i,s}$ | specific production rate of species $i$ at the surface ($mol\,m^{-3}\,s^{-1}$) |
| $Re$ | Reynolds number |
| $Sh$ | Sherwood number |
| $T$ | gas phase temperature (K) |
| $T_s$ | catalyst surface temperature (K) |
| $X_i$ | mole fraction of species $i$ ($mol\,mol^{-1}$) |
| $x$ | distance from the surface (m) |

*Greek letters*

| | |
|---|---|
| $\delta$ | film thickness (m) |
| $\Delta\tilde{H}_{CH_4}$ | partial oxidation reaction enthalpy per unit methane mole ($J\,mol^{-1}_{CH_4}$) |
| $\varepsilon$ | porosity |
| $\mu$ | gas viscosity ($kg\,m^{-1}\,s^{-1}$) |
| $\phi$ | Hatta number |
| $\psi$ | shape factor in the mass transfer coefficient equation |

*Subscripts*

| | |
|---|---|
| SR | steam reforming |
| b | bulk |
| CR | $CO_2$ reforming |
| g | gas phase |
| $i$ | generic species |
| max | maximum |
| p | particle |
| s | surface |
| WGS | water gas shift |

tion of experiments, which highlighted that the SCT-CPO system is controlled by heat and mass transfer and that the rate limiting step is the oxygen transport from the gas to the solid surface. Local temperature differences arise between the solid and the gas phase as a result of the transport phenomena limitations. The reactions remain largely confined at the catalyst surface with very high local temperatures, that are favourable to a fast and direct CO and $H_2$ production. These conclusions have been reached without detailing a complex micro-kinetic pathway but with a macro-kinetic description that includes rate expression parameters optimised on the experimental results obtained in our laboratories and presented in the literature [21,22]. Transport and thermodynamic properties of the gas system have been evaluated by means of Chemkin and transport libraries [23,24] and the contribution of homogeneous chemistry has been taken into account by means of GRI MECH 2.11 [25].

## 2. Experimental

The experimental set-up can be divided into four main sections: (1) mixing section, (2) reactor section, (3) gas cooling section, and (4) gas analysis section. In the first section, the feedstock is prepared by mixing and then fed to a tubular quartz reactor of 15 mm i.d. and 1.5 mm wall thickness. The catalyst is arranged in a fixed bed composed of 0.9 g of rhodium coated alumina spheres (approximately 275 spheres) of about 1.4 mm diameter. The catalyst bed is placed between two porous inert regions at the reactor inlet and outlet, which provide a shield for the radiant energy emerging from the active bed. The gas temperatures have been monitored by thermocouples located, respectively, before and after the inlet and outlet inert zones. The reactor set-up is equipped with an IR camera (Thermovision 900 SW/TE) for the measurements of the catalyst surface temperature in the fixed bed. The camera has an internal compensation and self-calibration system based on two micro black bodies and four temperature sensors. It is thermoelectrically cooled and operates in the short wave range 3–5 μm, suitable for high temperature applications. A filter "HT 1" (cut-on 3.82 μm, cut-off 3.9 μm) widens the measurement range to 2000 K. The system is also equipped with one 20° lens (field and view, $H \times V = 20^\circ \times 12.5^\circ$; spatial resolution 2.5 mrad) and one close-up lens (spatial resolution 0.32 mrad corresponding to about 250 μm). The IR camera is interfaced with a PC for the online acquisition of 12-bit digital images and data.

After the gas cooling section, where the condensation of the water present in the products is performed, a small amount of the gas stream is sampled and analysed with a gas chromatograph (HP 5890). Finally, the gas stream is collected in the vent line.

The ignition of the reactions is performed by warming up the catalyst bed with a hot air beam and by feeding the reactor with a pre-heated gas stream of methane and air at a $O_2$/C ratio below the stoichiometric value of 0.5. Once the start up procedure is complete, both the oven for the gas stream pre-heating and the hot air beam are removed, and the reactions remain self-sustained. The start up procedure takes

about 1 min and then the $O_2$/C ratio is gradually increased to the value of 0.5 to reach steady state conditions.

The gas hourly space velocity (GHSV) varied between 200 and 500 $N\,m^3\,kg_{cat}^{-1}\,h^{-1}$ with $O_2/C = 0.5$, $H_2O/C = 0$, $CO_2/C = 0$. The gas feedstock consisted of methane, containing a nitrogen amount of about 5%, and a $O_2$–$N_2$ mixture ($O_2$ = 70%) as the oxidant. Inlet gas temperature were always about 300 K and inlet pressure were between 1.3 and 1.5 atm.

## 3. Theoretical analysis methodology

In this work, the chemical reaction rates and the transport velocity of the reactants towards the catalyst surface have been compared. This comparison supports the interpretation of experimental data based on the occurrence of a transport-controlled regime, as it will be discussed in detail below.

The theoretical picture employed for this purpose consists of a diffusion–reaction system were mass and energy transfer are coupled with chemical reactions. The gas phase layer near the catalyst surface, where the transport phenomena take place, has been represented as a stagnant film close to a planar solid surface where heterogeneous chemical reactions occur. Eqs. (1) and (2) have been employed to describe the material balances across the film and the solid phase energy balance in steady state conditions:

$$k_{x,i}ac(X_{i,s} - X_{i,b}) = R_{i,s}, \quad \text{with } i = 1, \ldots, KK \tag{1}$$

$$ha(T_s - T) + \sum_{i=1}^{KK} R_{i,s} M_i \hat{H}_i = 0 \tag{2}$$

Gas phase compositions and temperatures have been considered as independent variables. Chemical species concentrations at the surface and the catalyst temperatures have been calculated as a result of the diffusion–reaction process described by Eqs. (1) and (2), varying the independent variables so as to cover the whole range of gas phase compositions and temperatures that can be encountered in the reactor.

The catalyst reactivity has been represented with three reactions (3)–(5):

$$CH_4 + 2O_2 \Rightarrow CO_2 + 2H_2O \tag{3}$$

$$2CH_4 + O_2 \Rightarrow 2CO + 4H_2 \tag{4}$$

$$CO + H_2O \Rightarrow CO_2 + H_2 \tag{5}$$

Arrhenius type expressions have been employed for the reaction rates and the kinetic constants have been optimised using literature reactivity data [21,22], developed in such experimental conditions that a kinetic-controlled regime is favoured. To this purpose, an implementation of a plug flow reactor model based on the Chemkin libraries has been employed, and a non-linear least-squares procedure was performed by a gradient method to optimise the kinetic constants. Details on expressions used in evaluating chemical kinetics are reported in the Chemkin documentation [24]. Table 1 includes the optimised activation energies and pre-exponential factors. Fig. 1a–c show comparisons between the experimental [21] and the calculated values; an analogous agreement has been obtained with results reported in reference [22]. It is noteworthy that the reaction rates of the surface reactions largely overcome the gas phase reaction rates estimated with the GRI MECH 2.11 mechanism [25] (see Fig. 2). This conclusion is in agreement with the considerations proposed in [11]. Considering the moderate importance of the gas phase chemistry at atmospheric pressure, also the enhancement of the mass transfer coefficients [26,27] throughout the film could be neglected. Another important factor that could be considered to support the minor importance of gas phase kinetics in fixed bed reactors for SCT-CPO of methane will be evident from the considerations on the transport-controlled regime presented below. As reported in detail in the following paragraphs, in fact, the transport limitations determine the occurrence of an inter-phase temperature difference between the gas and the solid phase. The gas phase, therefore, remains at by far lower temperatures than the solid, thus decreasing the importance of gas phase reactivity.

Table 1
Summary of kinetic Arrhenius parameters for reactions (3)–(5).

| Reaction | Pre-exponential factor ($m^6\,mol^{-2}\,s^{-1}$) | Activation energy ($J\,mol^{-1}$) |
|---|---|---|
| (3) | 2.3E+12 | 41860 |
| (4) | 2.15E+18 | 146510 |
| (5) | 3.7E+6 | 73210 |

The mass and heat transfer correlations employed in our calculations are those reported in [28], determined from experiments on fixed bed reactors. Several alternative equations have been tested [29], and all of them are substantially in agreement as concerns the transfer coefficients calculated with the correlation in [28]. Hence the equation for the mass transfer factor $J_D$ are:

$$J_D = 0.91\,Re^{-0.51}\psi, \quad 0.01 < Re < 50 \tag{6}$$

$$J_D = 0.61\,Re^{-0.41}\psi, \quad 50 < Re < 1000 \tag{7}$$

where $Re$ is a modified Reynolds number:

$$Re = \frac{Gd_p}{6\mu(1-\varepsilon)} \tag{8}$$

Moreover, since spherical catalyst particles have been used in our experiments, the shape factor, $\psi$, has been taken equal to 1 [30]. All the gas phase transport properties required in the calculations have been determined by the transport library of the Chemkin package [24]. The Chilton–Colburn analogy has been applied for the calculation of the heat transfer factors, $J_H$, from the mass transfer ones, $J_D$ [31].

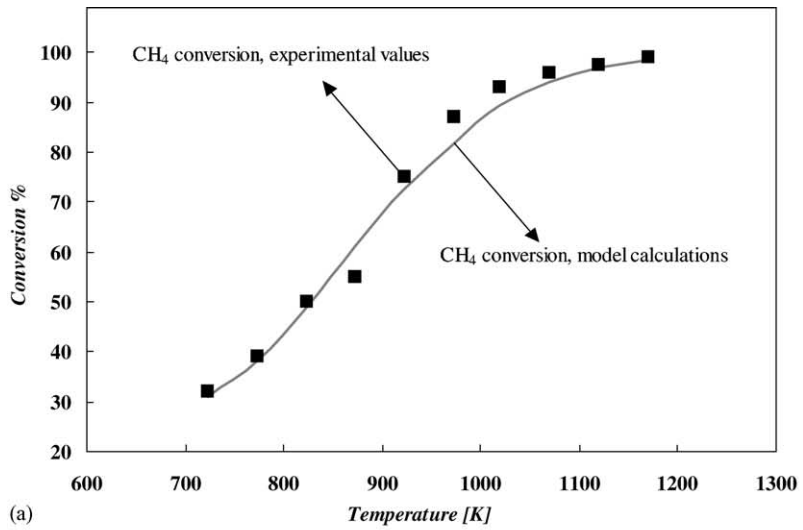


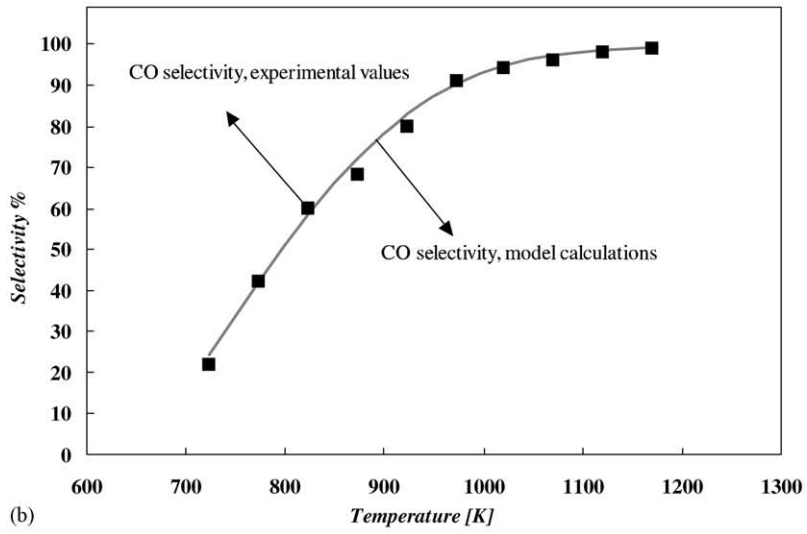


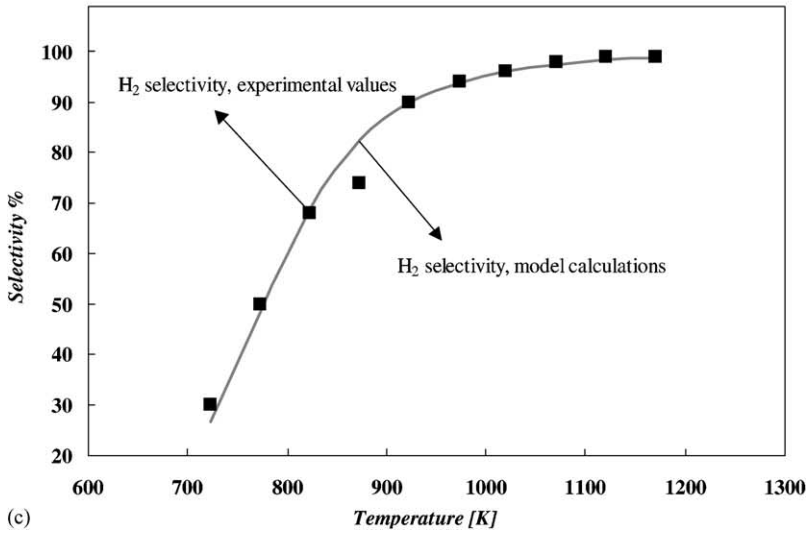


Fig. 1. Comparison between kinetic experimental data (symbols) and calculated values (lines): (a) methane conversion; (b) carbon monoxide selectivity; (c) hydrogen selectivity.

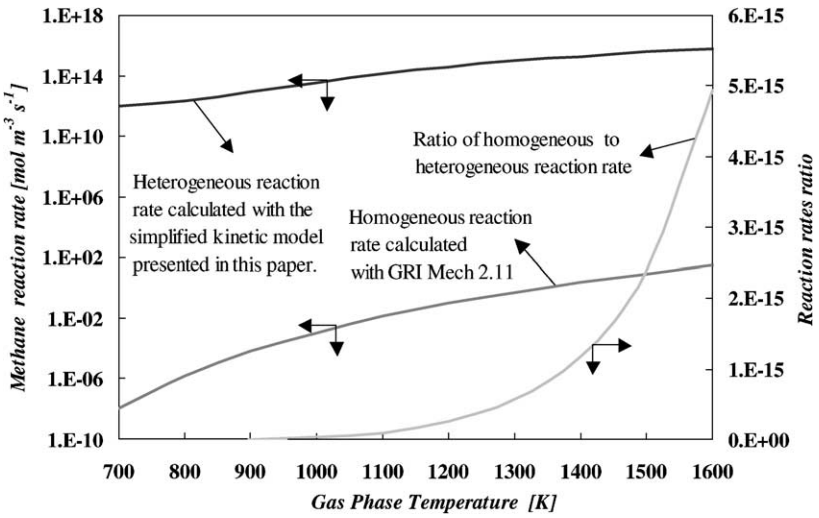


Fig. 2. Comparison between methane conversion rates due to heterogeneous and homogeneous chemistry. Calculations have been performed at the inlet conditions employed in the experiments.

## 4. Results and discussion

The experimental results are presented in Table 2 and Figs. 3–5. The data show that an increase in space velocity determines a rise in methane conversion and in the synthesis gas selectivity, an overall increase in the surface temperatures with a reduction of the temperature gradients in the axial direction and an increase in the gas outlet temperatures.

Eqs. (9)–(11) have been used to estimate the equilibrium temperatures ($T_{WGS}$, $T_{SR}$, $T_{CR}$), according to the procedures of reference [18], of every possible equilibrium that can be established in the reaction environment: the water gas shift

Table 2
Experimental results: methane conversion, $H_2$ and CO selectivities, gas outlet temperature and maximum catalyst temperature vs. space velocity

| GHSV ($N\,m^3\,kg_{cat}^{-1}\,h^{-1}$) | $CH_4$ conversion (%) | $O_2$ conversion (%) | CO selectivity (%) | $H_2$ selectivity (%) | $T_{gas}$ outlet (K) | $T_{solid}$ max (K) |
|---|---|---|---|---|---|---|
| 199.4 | 78.9 | 99.9 | 91.1 | 87.0 | 861 | 1283 |
| 301.1 | 83.0 | 99.8 | 93.0 | 88.3 | 917 | 1342 |
| 400.0 | 84.7 | 99.7 | 93.9 | 88.8 | 948 | 1364 |
| 500.0 | 85.0 | 99.6 | 94.3 | 88.5 | 972 | 1360 |

Operating conditions: $p_{gas,inlet} = 1.3$ atm, $T_{gas,inlet} = 298$–$308$ K, $m_{cat} = 0.9$ g, $O_2/C = 0.5$, $H_2O/C = 0$, $CO_2/C = 0$ (see Figs. 4 and 5).

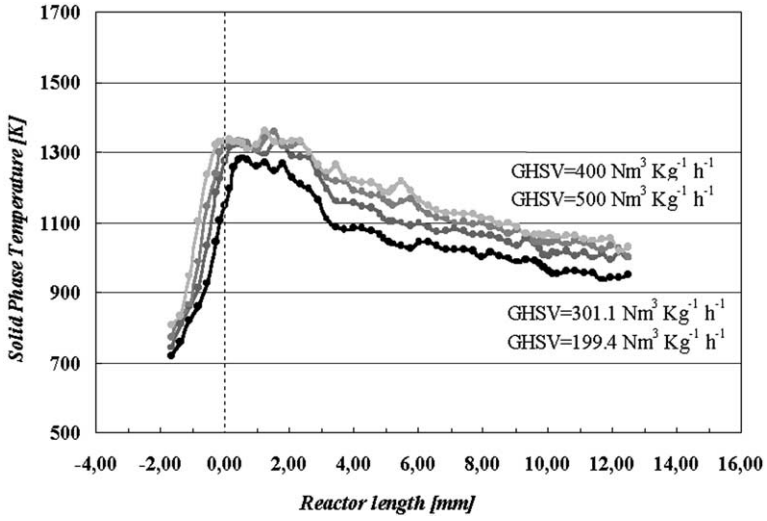


Fig. 3. Experimental axial profiles of the catalyst temperature at different space velocities.

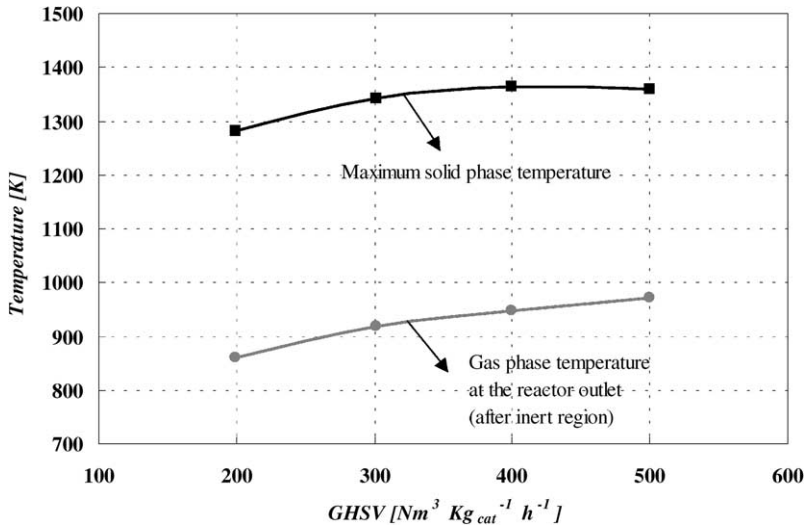


Fig. 4. Experimental values of both the gas temperatures at the reactor outlet and the maximum catalyst temperature vs. space velocity.

(5), the SR (12) and the $CO_2$ reforming (13) reactions.

$$T_{WGS} = \frac{-\Delta G_{WGS}}{R \ln(p_{CO_2} p_{H_2} / p_{CO} p_{H_2O})} \quad (9)$$

$$T_{SR} = \frac{-\Delta G_{SR}}{R \ln(p_{CO} p_{H_2}^3 / p_{H_2O} p_{CH_4})} \quad (10)$$

$$T_{CR} = \frac{-\Delta G_{CR}}{R \ln(p_{CO}^2 p_{H_2}^2 / p_{CO_2} p_{CH_4})} \quad (11)$$

$$CH_4 + H_2O \Rightarrow CO + 3H_2 \quad (12)$$

$$CH_4 + CO_2 \Rightarrow 2CO + 2H_2 \quad (13)$$

The calculated equilibrium temperatures (by employing partial pressure values of equations corresponding to experimental outlet compositions) have been compared with the measured values of the maximum catalyst surface temperature $T_{s,max}$ and with the experimental gas outlet temperatures $T_{gas,out}$. As already observed in other works [18,19] and in agreement with the results obtained by other authors with optical pyrometers [32–35], the aforementioned temperature values are ordered as follows:

$$T_{s,max} > T_{WGS} > T_{SR} \cong T_{CR} > T_{gas,out} \quad (14)$$

These results point out that the SCT-CPO system is not thermodynamically equilibrated and that the overall product mixture cannot be described as an equilibrium one. Moreover, it is confirmed that the reactions are mainly confined at the catalyst surface. Considering the remarkable activity of the rhodium catalysts, the very fast heterogeneous reactions could suffer from limitations exerted by transport phenomena (see Fig. 5), hence a transport-controlled regime can be

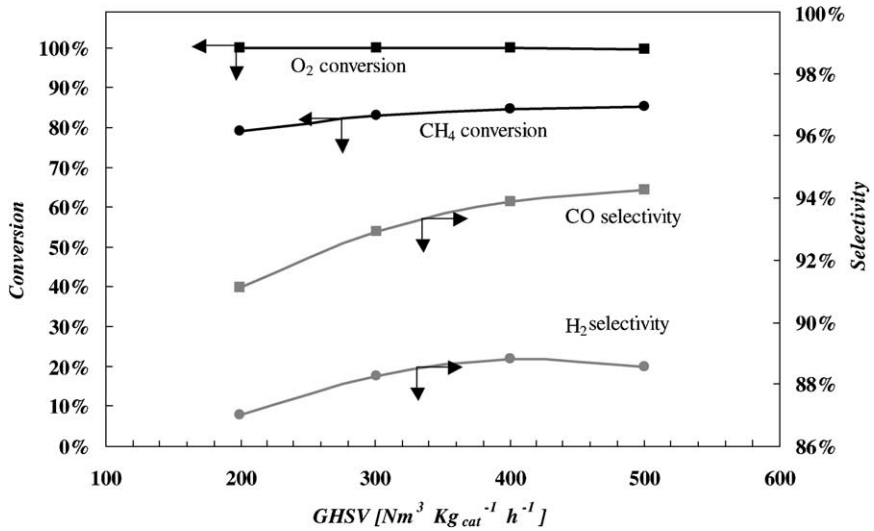


Fig. 5. Experimental values of $O_2$ and $CH_4$ conversion and of $H_2$ and CO selectivities vs. space velocity.

established. An increase in the space velocity determines, in fact, an improvement in the mass transfer coefficients of the reactants to the catalyst and, thus, the methane conversion, that is transfer limited, can rise (Fig. 5). The incomplete conversion of methane can be explained observing that the adopted oxygen to carbon ratio is equal to 0.5 and that $CO_2$ is present (it has been analytically determined) in the outlet gas phase.

By increasing GHSV, a net increase of the energy release in the solid phase takes place because of the rise of both methane conversion (%), and the gas mass flow rate fed to the reactor. This results in increasing temperatures, as it can be observed in the profiles in Fig. 3; similarly, the catalyst maximum temperature increases with space velocity (Figs. 3 and 4), together with the outlet gas temperature (Fig. 4), influenced by the solid phase.

The observed reduction of the axial surface temperature gradient with space velocity could be ascribed to more effective heat distribution through a particle-by-particle radiative mechanism, that becomes more and more intense at high surface temperatures, thus reducing the thermal gradient within the fixed bed.

The CO and $H_2$ formation is favoured at high temperatures [9,10,18,19], and hence the selectivity towards these products results increased at higher space velocities.

Similar experimental findings have been recently reported by Hohn and Schmidt [20]. However, these authors reported conversion and selectivity data but did not relate the reactivity features with experimental measurements of thermal profiles.

The solution of the diffusion–reaction Eqs. (1) and (2) sustains the presence of a transport-controlled regime. The calculation have indicated large differences in the reactant concentrations in proximity of the catalyst surface. More in detail, the calculations have shown (Fig. 6) that under all the tested conditions the oxygen mole fraction close to the catalyst surface resulted practically equal to zero. This result is typical of a transport-controlled system where relevant differences between mass transfer coefficients of reactants does exist. Indeed, the oxygen mass transport coefficient is much lower than that of methane.

It is noted that the reaction rates and stoichiometry determine the molar fluxes of the reactants towards the catalyst when a chemical reaction is the rate limiting step of a diffusive–reactive system (kinetic-controlled system). Instead, in a transport limited regime, with reaction rates considerably faster than transport velocities, the reactant fluxes achieve a maximum value that is not sufficient to feed the chemical reactions. This could determine a drastic reduction to values close to zero of the surface concentration of the species with the lowest mass transfer coefficient (the oxygen in the examined case). Clearly, in this situation the transport of the species with the lowest mass transfer coefficient, would also become the rate limiting step.

The relative weight of transport phenomena versus chemical reaction rates can also be analysed considering the case of a species $i$ moving across the film and reaching the catalyst surface where it reacts with a first-order equivalent reaction (Eq. (1)):

$$R_{i,s} = -k' c X_{i,s} \tag{15}$$

The comparison between the reaction and the transport velocity can be carried out by means of the dimensionless Sherwood ($Sh$) and superficial Damkohler ($Da_s$) numbers given by Eqs. (16) and (17):

$$Sh = \frac{k_{x,i}\, d_p}{D} \tag{16}$$

$$Da_s = \frac{k' d_p}{D} \tag{17}$$

that are representative of the coefficients for the transport process $k_{x,i}$ and the kinetic constant $k'$ of the surface reaction. Clearly, a kinetic-controlled regime takes place when

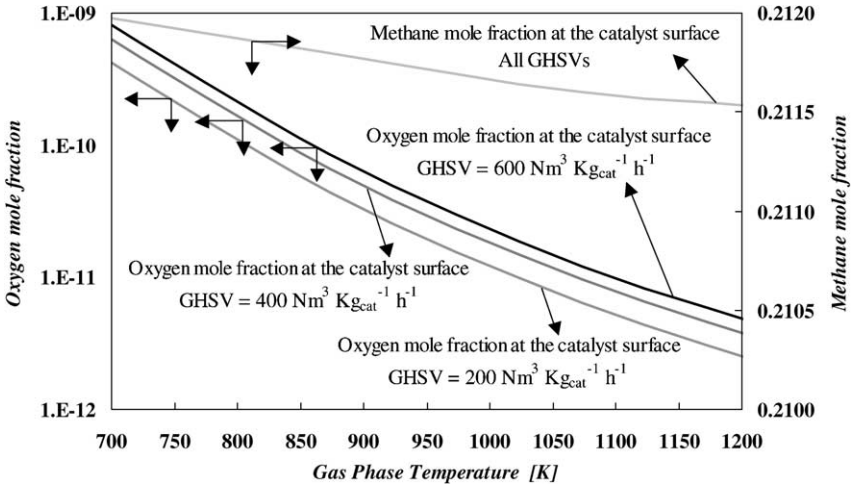


Fig. 6. Calculated methane and oxygen mole fractions on the catalyst surface at the inlet gas composition employed in the experiments.

$k_{x,i} \gg k'$ or when:

$$Sh \gg Da_s \tag{18}$$

On the other hand, in a transport-controlled regime:

$$Sh \ll Da_s \tag{19}$$

The following relationships provide a well known quantitative definition of the two regimes:

$$\begin{array}{ll} \text{Kinetic-controlled regime :} & Sh > 10\,Da_s \\ \text{Transport-controlled regime :} & Sh < 0.1\,Da_s \end{array} \tag{20}$$

We have calculated an equivalent first-order kinetic constant on the basis of the solution of the diffusion–reaction problem in the range of operating conditions investigated and we have estimated the ratios between $Sh$ and $Da_s$ numbers using the calculated $X_{O_2,s}$ values shown in Fig. 6. Fig. 7 includes the results and shows that the SCT-CPO conditions largely fell inside the area characterised by a transport-controlled regime. The data points drawn in Fig. 7 have been estimated at three different GHSV values (determined at constant catalyst volume) and at six temperatures. These data points indicate that at constant GHSV, the temperature increase rises the reaction rate more than the transport velocity; while at constant temperature, a space velocity increase slightly shifts the system towards the kinetic-controlled regime area that, however, remains quite far.

Moving from mass to heat transfer considerations, it is noted that the energy released by the exothermic surface reactions must be transferred to the gas bulk phase and, therefore, a temperature difference between the catalyst and the gas appears. This difference stabilises at values determined by the heat transfer coefficients and by the net energy flux to be transferred to the bulk gas phase. Consequently, the catalyst operates at temperatures higher than those of the gas phase, and this favours the selective and fast formation of the partial oxidation products [18,19].

A qualitative investigation of the parameters that influence the solid–gas temperature difference has been carried out assuming that only the partial oxidation (4) takes place at the catalyst surface. This assumption provides a conservative estimation of the surface temperature, below the expected values, since the partial oxidation is by far less exothermic than total oxidation. In this case, the energy balance Eq. (2) can be simplified with Eq. (21) as:

$$(T_s - T) = 2\frac{k_{x,O_2}}{h} c (X_{O_2,b} - X_{O_2,s})(-\Delta \tilde{H}_{CH_4}) \tag{21}$$

where it can be noticed that $X_{O_2,s}$ is always nearly 0 (Fig. 6).

The inter-phase temperature difference depends on the mass to heat transfer coefficients ratio and, therefore, the effect of the space velocity on $(T_s - T)$ is negligible, because the transfer coefficients increase simultaneously with the Reynold number, as a result of the Colburn analogy.

Solid–gas temperature differences along the bed depend on the variation of the gas phase composition. This effect has been analysed utilising the percentage of methane conversion into synthesis gas as a variable indicative of the compositional change along the bed, i.e. a 0% methane conversion would correspond to the inlet composition, whereas 50% conversion would correspond to a mixture where half of the initial amount of methane is unreacted and the other half has been transformed into CO and $H_2$.

Fig. 8 shows the surface temperatures, calculated with the reaction set represented by Eqs. (3)–(5), that as expected do not depend on the space velocity and that evolve towards the gas phase temperature with increasing methane conversion. Therefore, in a fixed bed reactor we may expect that the temperature difference between the solid surface and the gas phase, that should be independent on the space velocity, should have a maximum near the reactor entrance and should reduce along the bed as the reaction approaches to completion.

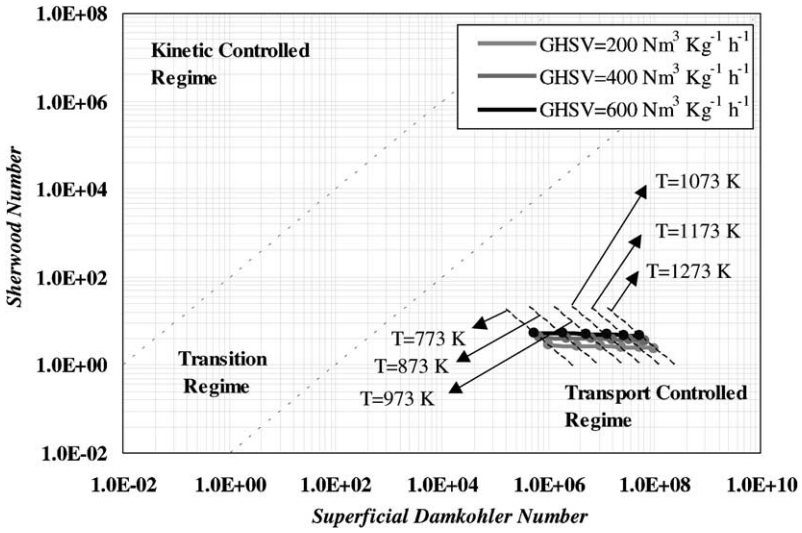


Fig. 7. Reactor operating regimes map.

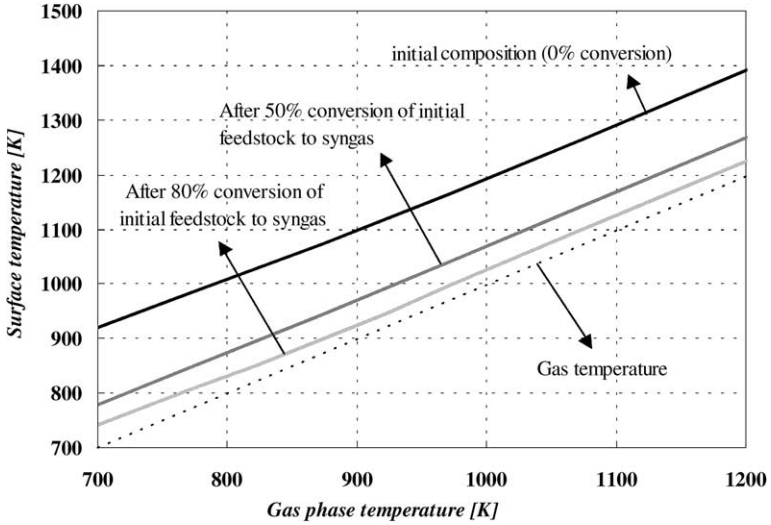


Fig. 8. Calculated temperature difference between the catalyst and the gas bulk phase valid for all the GHSV values examined.

## 5. Summary and conclusions

This work presents experimental data of catalytic partial oxidation of methane over a rhodium catalyst in a fixed bed reactor. The data show that methane conversion increases with space velocity, together with the catalyst surface temperature, the gas phase outlet temperature and the selectivity towards partial oxidation products. The experimental data are discussed considering that very fast and selective reactions are largely occurring at the solid surface. A theoretical analysis indicates that SCT-CPO occurs in transport-controlled regime, where oxygen transport from the gas phase to the catalyst surface is the rate limiting step. Along the catalytic bed, a temperature difference between the catalyst surface and the gas phase is expected, that should be independent on space velocity and dependent on the feedstock conversion to syngas. Methane conversion increases with space velocity, as an effect of improved transport coefficients. Due to the occurrence of extremely fast heterogeneous reactions, gas phase reactions do not affect the overall reactivity. A mathematical model of the SCT-CPO reactor based on these conclusions is under development.

## References

[1] A. Chauvel, G. Lefebvre, Synthesis gas derivatives and major hydrocarbons, in: Petrochemical Processes Technical and Economical Characteristics, Vol. 1, Editions Technip, Paris, 1989, pp. 27–116.
[2] B. Elvers, S. Hawkins, M. Ravenscroft, J.F. Rounsaville, G. Shulz (Eds.), Ullman's Encyclopaedia of Industrial Chemistry, VCH, Weinheim, 1989, pp. 186–214.
[3] J.R. Rostrup-Nielsen, Catalytic steam reforming, in: J.R. Anderson, M. Boudardt (Eds.), Catalysis Science and Technology, Vol. 5, Springer, Berlin, 1984, pp. 1–118.
[4] T.S. Christensen, I.I. Primdhal, Hydrocarbon Process. Int. Ed. 73 (1994) 39.
[5] J.R. Rostrup-Nielsen, Catal. Today 18 (1993) 305.
[6] Ib Dybkjaer, Fuel Process. Technol. 42 (1995) 85.
[7] V.R. Choudary, A.S. Mamman, S.D. Sansare, Angew Chem., Int. Ed. Engl. 31 (1992) 1189.
[8] H. Hickman, L.D. Schmidt, J. Catal. 138 (1992) 267.
[9] O. Deutschmann, L.D. Schmidt, Proc. Comb. Inst. 27 (1998) 2283.
[10] A.S. Bodke, S.S. Bharadwaj, L.D. Schmidt, E. Ranzi, Science 285 (1999) 712.
[11] O. Deutschmann, L.D. Schmidt, AIChE J. 44 (1999) 2465.
[12] O. Deustchmann, R. Schwiedernoch, L.I. Maier, D. Chatterjee, Stud. Surf. Sci. Catal. 136 (2001) 251.
[13] S.S. Bharadwaj, L.D. Schmidt, Fuel Process. Technol. 42 (1995) 109.
[14] D. Dissanake, M.P. Rosinek, J.H. Lunsford, J. Phys. Chem. 97 (1993) 3644.
[15] D.A. Hickman, L.D. Schmidt, Science 259 (1993) 343.
[16] Y. Matsumura, J.B. Moffat, Catal. Lett. 24 (1994) 59.
[17] D.K. Zerkle, M.D. Allendorf, M. Wolf, O. Deutschmann, J. Catal. 196 (2000) 18.
[18] L. Basini, A. Guarinoni, A. Aragno, J. Catal. 190 (2000) 284.
[19] L. Basini, K. Aasberg-Petersen, A. Guarinoni, M. Ostberg, Catal. Today 64 (2001) 9.
[20] K.L. Hohn, L.D. Schmidt, Appl. Catal. A: Gen. 211 (2001) 53.
[21] A. Beretta, G. Groppi, L. Maiocchi, P. Forzatti, Appl. Catal. A: Gen. 187 (1999) 49.
[22] P.D. F Vernon, M.L.H. Green, A.H. Cheetham, A.T. Ashcroft, Catal. Lett. 6 (1990) 181.
[23] R.J. Kee, G. Dixon Lewis, J. Warnatz, M.E. Coltrin, J.A. Miller, A Fortran Computer Package for the Evaluations of Gas Phase Multi-Component Transport Properties, Sandia National Laboratory, SAND86-8246, 1986.
[24] R.J. Kee, F.M. Rupley, J.A. Miller, Chemkin II: A Fortran Chemical Kinetic Package for the Analysis of Gas Phase Chemical Kinetics, Sandia National Laboratory, SAND86-8246, 1989.
[25] C.T. Bowman, R.K. Hanson, D.F. Davidson, W.C. Gardiner Jr., V. Lissianki, G.P. Smith, D.M. Golden, M. Frenklach, M. Goldenberg, GRI MECH 2.11, http://www.me.berkeley.edu/gri_mech, 1995.
[26] D.E. Rosner, Transport Processes in Chemically Reacting Flow Systems, Butterworths, Stoneham, MA, 1986.
[27] L.D. Pfefferle, Catal. Today 26 (1995) 255–265.
[28] F. Yoshida, D. Ramaswami, O.A. Hougen, AIChE J. 8 (1962) 5.
[29] R.H. Perry, D.W. Green, Perry's Chemical Engineers' Handbook, 7th Edition, 1998.
[30] B. Gamson, Chem. Eng. Prog. 47 (1951) 19.

[31] T.H. Chilton e, A.P. Colburn, Ind. Eng. Chem. 26 (1934) 1183.
[32] D. Dissanake, M.P. Rosinek, J.H. Lunsford, J. Phys. Chem. 97 (1993) 3644.
[33] Y.F. Chang, H. Heinemann, Catal. Lett. 21 (1993) 215.
[34] Y. Matsumura, J.B. Moffat, Catal. Lett. 24 (1994) 59.
[35] F. Basile, L. Basini, M. D'Amore, G. Fornasari, A. Guarinoni, D. Matteuzzi, G. Del Piero, F. Trifirò, A. Vaccari, J. Catal. 173 (1998) 247.